scientific reports

Check for updates

OPEN

Targeting LAG3 to alter the tumor immune reactivity of CD8+T cells is a potential therapy for skin cutaneous melanoma

Jin Gong✉, Yan Zhao, Shaozhi Gong, Chunyu Deng & Yajie Zhou

CD8⁺ T cells exert a significant effect in immune infiltration, drug resistance and cell survival in cancers, but the roles and mechanisms in skin cutaneous melanoma (SKCM) remain unclear. In the present study, prognostic biomarkers associated with CD8⁺ T cell subsets were screened, and the significance of CD8⁺ T cells in SKCM immunotherapy was explored by integrated single-cell RNA sequencing (scRNA-seq) and Bulk RNA sequencing (Bulk RNA-seq) analyses. Based on scRNA-seq analysis, CD8 + T cells were divided into two subgroups: CD8 + LAG3 + T cells and CD8 + LAG3-T cells. Cell-cell communication analysis revealed that both subsets closely interact with melanoma cells. Differential gene expression analysis showed that LAG3 was up-regulated in SKCM, and immune infiltration analysis showed that the survival prognosis was significantly better in the Score-High group than in the Score-Low group. Assay results demonstrated that both the LAG3 inhibitor ZYF0033 and the monoclonal antibody Miptenalimab significantly suppressed tumor proliferation and metastasis, while enhancing immune cell infiltration in murine models. This study revealed the functional heterogeneity of CD8 + T cells in SKCM and demonstrated that LAG3 inhibition suppresses tumor proliferation and metastasis. Moreover, reduced LAG3 expression significantly enhanced CD8 + T cell immune infiltration, highlighting the regulatory role of LAG3 in CD8 + T cell function within the tumor microenvironment. These findings provided further evidence that SKCM may be effectively treated by targeting LAG3.

Keywords scRNA-seq, Bulk RNA-seq, CD8⁺ t cells, LAG3, Immunotherapy

Skin cutaneous melanoma (SKCM) is a malignant tumor that occurs in skin melanocytes, and its incidence has been gradually increasing in recent years, making it an additional threat to human health[1]. Patients are usually diagnosed with SKCM at an advanced stage, resulting in a poor prognostic overall survival (OS) that varies widely across regions and ethnicities[2,3]. Due to the aggressive and metastatic features of malignant SKCM, metastasis of cancer cells cannot be prevented even by total excision. Some reports have shown that genomic profiles are helpful to identify genetic susceptibility genes for SKCM and that the prognosis of SKCM can be significantly improved by immunotherapy[4].

In recent years, immunotherapy has become an emerging research area in anticancer therapy. Immune checkpoint inhibitors (ICIs), which have been shown to be effective against a variety of solid tumors, exert its effect mainly through the infiltration of effector T cells into the tumor microenvironment (TME)[5–7], while the cytotoxic T cell infiltration has been reported to be correlated with the prognosis of SKCM patients[8]. Thus, tumor cells can be cleared by activating T cell response to improve patient survival[9]. CD8⁺ T cells being classical tumor-reactive T cells play a prominent role in immune infiltration, drug resistance and survival in cancer[10]. Activated naive CD8⁺ T cells will be differentiated into mature effector CD8⁺ T cells, which can effectively clear antigens and inhibit infection[11]. Mediated by genetic behaviors such as extracellular metabolites and immune signaling, CD8⁺ T cells further adapt to the changing immune microenvironment to guarantee CD8⁺ T cell-mediated immunity[12]. In addition, several studies have suggested that the extent of CD8 + T cell infiltration is associated with alterations in gene expression, which may influence the metastatic potential of SKCM[13,14]. Therefore, an in-depth study of the effects and mechanisms of CD8⁺ T cells in SKCM is essential for the clinical outcome of patients.

Department of Dermatology, The First Affiliated Hospital of Yangtze University, The First People's Hospital of Jingzhou, No. 55, Jianghan North Road, Shashi District, Jingzhou 434000, Hubei, China. ✉email: 2022721085@yangtzeu.edu.cn

In response to sustained tumor antigen stimulation, expression of cytotoxic T lymphocyte antigen-4 (CTLA-4) and lymphocyte activation gene 3 (LAG3), which have been reported to be associated with the immune response to SKCM, is elevated on activated $CD8^+$ T cells. CTLA-4 (Ipilimumab), a targeted drug earlier approved by the Food and Drug Administration (FDA) for immunotherapy in SKCM, blocks T cell activation signaling by competitively binding to CD28[15]. Unlike the mechanism of CTLA-4, LAG3 can inhibit T cell activation by reducing signaling through the T cell receptor (TCR)[16]. On activated $CD8^+$ T cells, LAG3 expression causes T cell dysfunction and inhibits the proliferation of activated T cells[17]. Although LAG3 (Relatlimab) has been approved by the FDA as an ICIs for the treatment of malignant SKCM in May 2022, insights into the immunomodulation of LAG3 on $CD8^+$ T cells in SKCM are still of research significance.

A study by Yan Min et al. has revealed the functional heterogeneity of T cells in SKCM using single-cell RNA sequencing (scRNA-seq). The association of T cell infiltration with prognostic survival was assessed by constructing tumor-reactive T cell signatures (TRS) to observe the ability of TRS to predict immunotherapy in SKCM patients[18]. In the present study, $CD8^+$ T cell subsets with heterogeneity of LAG3 expression in SKCM were identified, $CD8^+$ $LAG3^-$ T cell-related prognostic biomarkers were screened, and immunotherapy responsiveness were predicted by comprehensive analysis of scRNA-seq and Bulk RNA sequencing (Bulk RNA-seq) data.

Data and methods

Data sources

The SKCM scRNA-seq data were selected from the GSE215120 dataset in the Gene Expression Omnibus (GEO), of which three SKCM samples (GSM6622299, GSM6622300, GSM6622301) were selected for data analysis. The TCGA-SKCM data from The Cancer Genome Atlas (TCGA) was selected as the training set for Bulk RNA-seq, and only the samples with OS were retained, totaling 447 cancer samples. 556 normal tissue samples were obtained from Genotype-Tissue Expression (GTEx). The validation sets were selected from two datasets GSE54467 and GSE65904 from GEO, including 79 and 210 SKCM samples, respectively.

scRNA-seq

The scRNA-seq dataset of 3 SKCM samples from GSE215120 was preprocessed using the R package Seurat (v4.1.0). Three samples were merged and batch effect correction was performed using CCA to eliminate invalid cells and genes. Quality control of the integrated dataset was conducted to retain cells with at least 100 detected genes and a minimum number of UMIs. Additionally, cells with over 25% mitochondrial gene content were excluded to ensure data integrity. Highly variable genes (HVGs) between cells were identified and principal component analysis (PCA) was performed on the normalized data. Based on the first 50 principal components, the FindNeighbors function was applied to identify neighboring cells, followed by clustering using the FindClusters function. The resulting cell populations were visualized via UMAP. Cell clusters were annotated according to the expression profiles of known marker genes. Intercellular communication networks were inferred using the R package CellChat 1.6.1.

Enrichment analyses

Marker genes of $CD8^+$ $LAG3^-$ T cells were selected for gene ontology (GO) term and Kyoto Encyclopedia of Genes and Genomes (KEGG) pathway enrichment analyses by the R package clusterprofiler, screening GO terms or KEGG signaling pathways with $P < 0.05$[19–21].

Differential gene expression analysis

The TCGA-SKCM samples ($N = 447$) and GTEX normal tissue samples ($N = 556$) were subjected to differential gene expression analysis using the limma-3.54.1 package, with $|\log_2(\text{fold change, FC})| > 2$, and adj. $P < 0.05$ as the parameters. The differentially expressed genes (DEGs) distribution was demonstrated by volcano plots drawn with the R package ggplot2.

Immune infiltration analysis

The immune cell infiltration scores in the TCGA-SKCM and GTEX samples were calculated using the CIBERSORT algorithm (https://cibersortx.stanford.edu/), with the expression matrix of DEGs as data. According to the median value of the extracted scores, the TCGA-SKCM samples were categorized into the Score-High and Score-Low groups. Heatmap of immune infiltration was plotted using R package Pheatmap. Immune infiltration scoring was performed using the R package ESTIMATE. StromalScore, ImmuneScore, ESTIMATEScore and tumor purity were calculated using the single-sample gene set enrichment analysis (ssGSEA) algorithm.

Survival analysis

Survival analysis was performed using the R package Survival. Differences in OS and disease-specific survival (DSS) for different groups of patients were demonstrated using the Kaplan-Meier (KM) curves plotted by the R package Survminer. Receiver operating characteristic (ROC) curves were plotted using the R package timeROC.

Weighted gene co-expression network analysis (WGCNA)

The gene expression matrix of TCGA-SKCM was selected for WGCNA, and the top 25% genes were retained according to the obtained median absolute deviation (MAD), with the soft threshold set at 0.8. $CD8^+$ T immune infiltration group (high vs. low), age (>=60 vs. <60), sex (male vs. female), cancer stage (I/II vs. III/IV), metastasis (M1 vs. M0) and other traits were selected as grouping data. All genes were classified into different color modules according to their correlation with the traits, and the gene modules with the highest correlation coefficients were selected for subsequent analyses.

Least absolute shrinkage and selection operator (LASSO)

Univariate Cox regression models were established using the Coxph function of the R package Survival, and the prognosis-related chemokine-related genes were screened according to $P < 0.05$. The regression coefficients of the variables were compressed using the LASSO algorithm in the R package glmnet, and the signature Score of the patients was calculated according to the gene expression and their corresponding regression coefficients:

$$Score = \sum {}^{n}_{i=0} \beta\, i * \chi\, \mathrm{i}*$$

βi: Weight coefficient of each gene; χi: Expression of each gene.

The risk score of each sample was calculated according to the formula, and the samples were assigned to the High-risk and Low-risk groups by the median value.

Treatment and chemotherapy sensitivity analysis

Similarity of expression profiles between SKCM and immunotherapy patients was measured using Submap. According to cell line expression data and drug response information from the GDSC2 (http://www.cancerrxgene.org) database, combined with TCGA-SKCM expression profiles, the difference between the $\log_2$ (IC50) of individual drugs for a variety of cell lines in the GDSC2 database and the High-/Low-risk groups was predicted using the R package oncoPredict.

Mouse modeling treatment

SPF-grade male C57BL/6 mice of 5–6 weeks were purchased from Jiangsu GemPharmatech Co., Ltd. and B16F10 cells (Procell, CL-0319) were purchased from Procell Co., Ltd. The cells were resuspended in 100 μL PBS and injected subcutaneously into the right axilla of mice. A total of 12 mice were enrolled in the modeling assay, and tumor growth was observed twice a week, with a volume of more than 50 mm^3 considered as successful modeling. LAG3 inhibitor ZYF0033 (MCE, HY-144088) or monoclonal antibody Miptenalimab (BI-754111, MCE, 0HY-P99736) was dissolved with DMSO according to the studies by Jingwen Si et al.[22] and Markus Zettl et al.[23]. Mice were randomly divided into 3 groups on day 11 after cell inoculation, which was redefined as day 0. The ZYF0033 group (N = 4) and the Miptenalimab group (N = 4) were injected intraperitoneally with 10 mg/kg ZYF0033 or Miptenalimab, respectively, and the DMSO group (N = 4) was injected intraperitoneally with an equal amount of DMSO solution. The drugs were administered once a week for 6 weeks and observed twice a week. Mice were executed via cervical dislocation at the end of modeling, extracting tumor tissues for subsequent assays. And the animal experiments were approved by the Animal Ethics Committee of the Yangtze University. All operating methods were performed in accordance with relevant guidelines and regulations. All methods reported were in accordance with ARRIVE guidelines.

Xenograft mouse models

B16F10 cells were resuspended in 100 μL PBS and injected into mice by tail vein. On day 11 after cell inoculation, the mice were randomly divided into 3 groups and treated with ZYF0033, Miptenalimab or DMSO as described above. Mice were imaged using the VivoVision Systems Lumazone (Mag Biosystems, Tucson, AZ, USA) on day 7 and 14 after injection.

In vivo tumor formation assay in mice

Tumor diameters and lengths were measured every 7 days after successful modeling, repeated 3 times, and the tumor volume was calculated according to the formula "tumor volume (mm^3) = 0.5×(tumor long diameter×tumor short diameter^2)". Tumor growth curves were calculated based on the tumor weight, which was measured every 2 days.

Hematoxylin-eosin (H&E) staining

The extracted mouse tumor tissues were made into 3-μm-thick paraffin sections and separately stained with hematoxylin solution and eosin according to the kit protocols. Sealing with clear neutral gum, the sections were observed using a light microscope for the pathological morphology of the tissue cells.

Immunohistochemical assay

The paraffin sections of SKCM tissues were dehydrated and immersed in citrate buffer for antigen repair. The sections were washed with PBS and incubated in 3% H_2O_2 for 30 min at room temperature away from light. After PBS washing, the sections were closed with 3% BSA for 30 min. Ki67 rabbit monoclonal antibody (Beyotime, AF1738) or other primary antibodies was added to the sections and incubated overnight at 4℃ away from light. After washing, horseradish peroxidase (HRP)-labeled secondary antibody was added and incubated at room temperature for 1 h. Staining was visualized under a light microscope using the substrate DAB. Primary antibodies include: LAG3 rabbit monoclonal antibody (abcam, ab209236), SAMD3 rabbit polyclonal antibody (abcam, ab84177), SAMSN1 rabbit polyclonal antibody (ThermoFisher, PA5-82571), TRIM22 rabbit polyclonal antibody (abcam) ab224059), CTLA4 rabbit monoclonal antibody (abcam, ab237712), CD8 rabbit monoclonal antibody (abcam, ab217344).

Statistical analysis

Data in the present study were calculated using the GraphPad Prism, with the expression of mean ± standard deviation (SD). Data between multiple groups were analyzed using ANOVA test and differences between two groups were analyzed using t-test. $P < 0.05$ was statistically significant.

Results

Identification of six immune cell subsets in SKCM

The original dataset comprising three samples was merged, and batch effect correction was performed using CCA, resulting in 28,812 cells and 22,780 genes (Supplementary Fig. 1A, B). Following quality control filtering, the dataset retained 27,748 cells and 22,780 genes (Supplementary Fig. 1C, D). Hypervariable genes were identified and visualized via eigenvariance plots. Principal component analysis (PCA) was then conducted, and the top 50 principal components were selected for downstream analyses (Supplementary Fig. 1E, 1 F). A total of 27 distinct cell populations were subsequently visualized using UMAP (Fig. 1A, B). Cells were annotated according to the expression of the 18 marker genes in different cell clusters, obtaining 7 major identified cell types: B Cell, Endothelial, Fibro, Melanoma, Monocyte&Macrophage (Mono&Macro), NK Cell (NK), T Cell. (Fig. 1C, D). Subsequently, the above annotated immune cell types (T Cell, B Cell, NK, Mono&Macro) were extracted and re-annotated, obtaining 6 cell types: B Cell, $CD4^+$ T, $CD8^+$ T, cell cycle T, Mono, NK (Fig. 1E, F).

Immunomodulatory effects of LAG3 on $CD8^+$ T cells

To further explore the immunomodulatory effects of LAG3 on $CD8^+$ T cells in SKCM, $CD8^+$ T cell subsets were further annotated using marker genes such as LAG3, CTLA-4, and so on, obtaining two subsets, $CD8^+$ $LAG3^+$ T cells and $CD8^+$ $LAG3^-$ T cells (Fig. 2A, B and C). Subsequently, the probability of communication between each subset was calculated, and the results showed that both $CD8^+$ $LAG3^+$ T cells and $CD8^+$ $LAG3^-$ T cells interacted with Melanoma cells, and the interaction between the Melanoma subgroup and CD8 + LAG3-T and CD8 + LAG3 + T was comparable (Fig. 2D). Since previous studies have shown that LAG3 inhibitors are effective against melanoma, we selected a subset of CD8 + LAG3-T cells for subsequent analysis.

Functions and pathway analysis of $CD8^+$ $LAG3^-$ T cell-associated marker genes

GO term or KEGG pathway enrichment analyses of the 2,314 marker genes obtained from $CD8^+$ $LAG3^-$ T cells showed that they were significantly enriched in biological processes (BPs) such as positive regulation of cell adhesion, regulation of T cell activation, cellular components (CCs) such as melanosome, pigment granule, and ribosome, and molecular functions (MFs) such as actin binding, cadherin binding, DNA-binding transcription

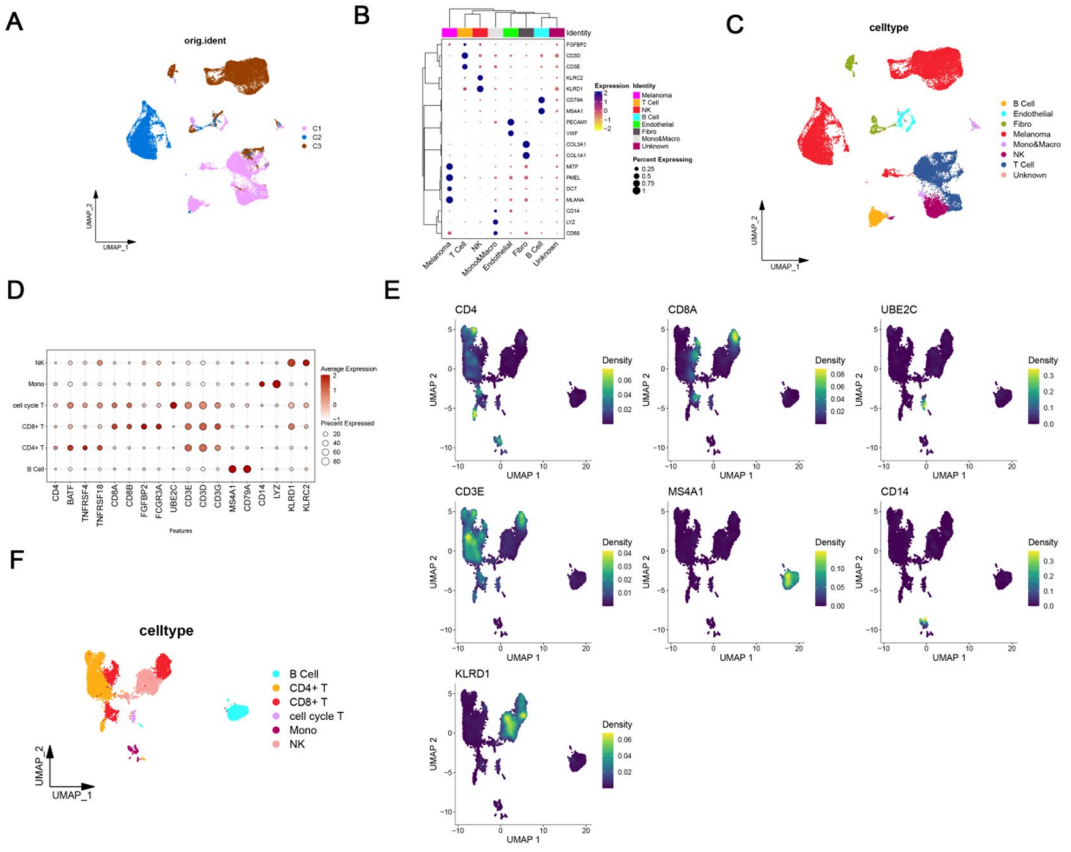

Fig. 1. Identification of different types of cell clusters based on scRNA-seq data. (**A**) UMAP plot presented cell clusters in different samples; (**B**) bubble plots of markers used for cellular annotation; (**C**) UMAP presented cellular annotation results; (**D**) bubble plots of markers used for immune cell subset annotation; (**E**) highlighted maps of classic markers of various immune cell subsets; (**F**) UMAP plot presented immune cell subset annotation results.

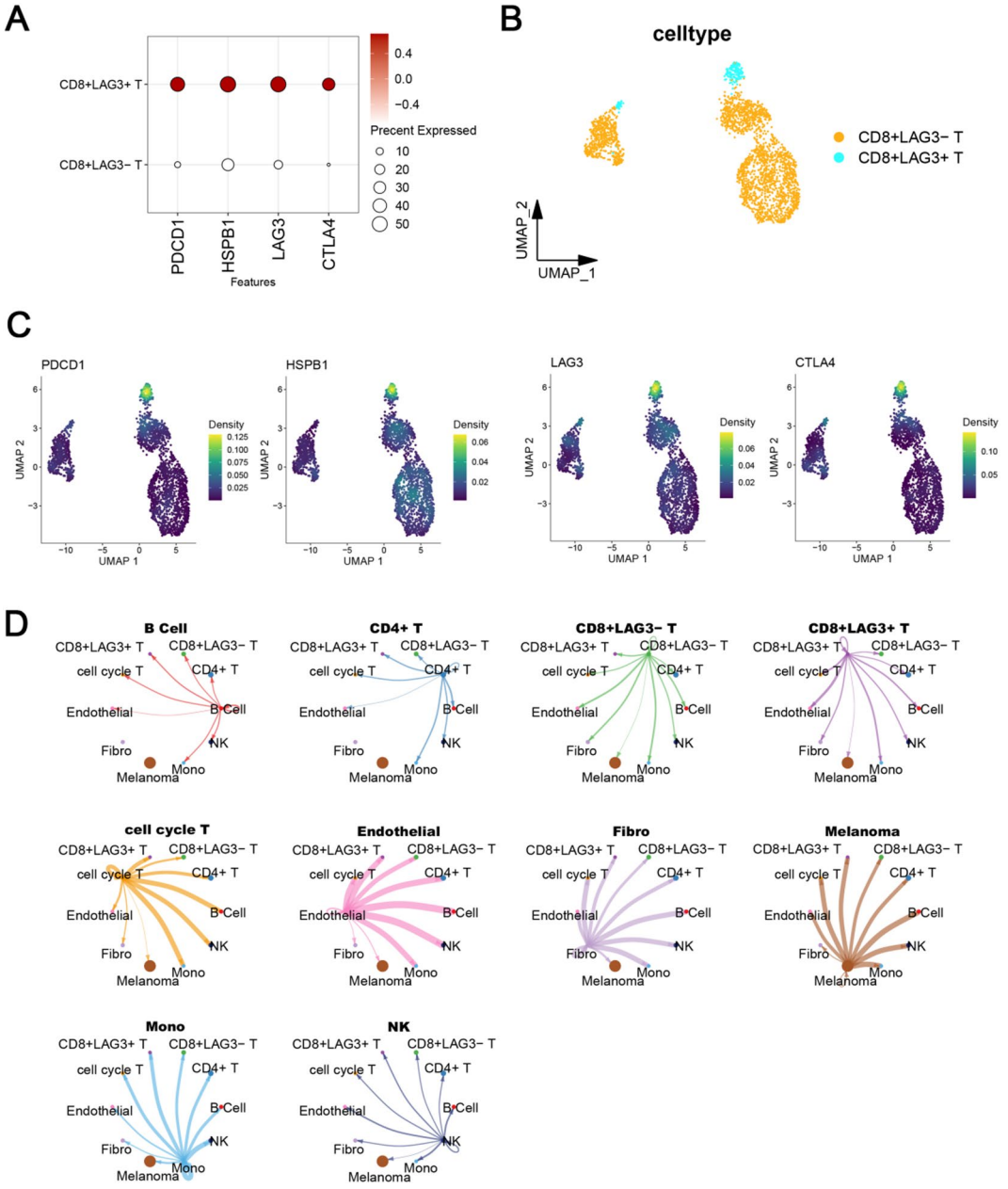

Fig. 2. Immune cell subset annotation and cellular communication. (**A**) Bubble plots of marker genes used for CD8$^+$ T cell subset annotation; (**B**) UMAP plots demonstrated the results of CD8$^+$ T cell subset annotation; (**C**) highlighted plots of the expression of marker genes used for CD8$^+$ T cell subset annotation; (**D**) plots of cellular interaction networks.

factor binding (Fig. 3A-C). In addition, the marker genes were also related to signaling pathways such as Oxidative phosphorylation, PI3K-Akt signaling pathway, and chemokine signaling pathway (Fig. 3D).

CD8$^+$ T cell-related gene modules identified by WGCNA

There were 1,313 up-regulated and 3,436 down-regulated genes obtained by differential gene expression analysis, of which LAG3 expression was up-regulated in tumors (Fig. 4A). Immune cell infiltration in TCGA-SKCM and GTEX samples was demonstrated via stacked plots (Fig. 4B), and the TCGA-SKCM samples were categorized into the Score-High and Score-Low groups based on the median scores of CD8$^+$ T cell immune infiltration. The KM curves showed that the prognosis survival of the Score-High group was significantly better (Fig. 4C). The genes associated with the clinical features were subsequently clustered using WGCNA, and the heatmap demonstrated the relationship and significance values between each clinical feature and gene module (Fig. 4D). Of all the gene modules, the one with the highest correlation with CD8$^+$ T cells was turquoise, containing 427 genes, shown in supplementary Table 1 for details (Fig. 4E, F).

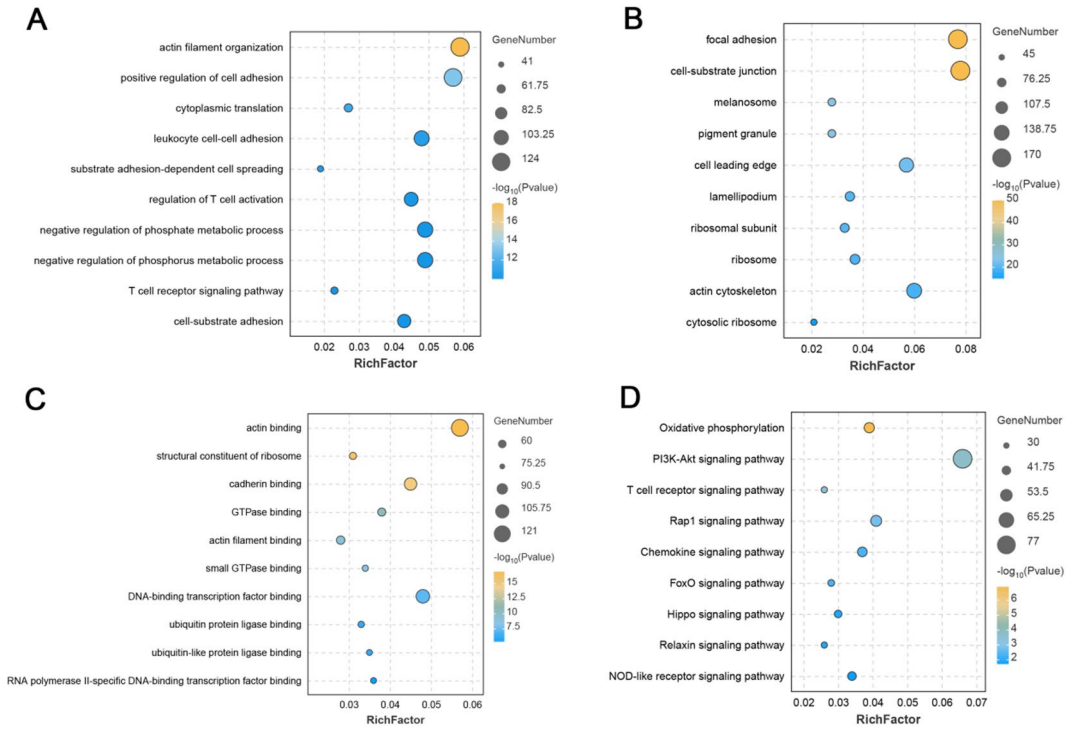

Fig. 3. Enrichment analyses of CD8$^+$ LAG3$^-$ T cell markers. (**A**) Top 10 significant BPs; (**B**) Top 10 significant CCs; (**C**) Top 10 significant MFs; (**D**) Top 10 significant KEGG signaling pathways.

SKCM patients with high risk scores had a poorer prognosis

There were 112 genes obtained by taking the intersection between the 760 marker genes from CD8$^+$ LAG3$^-$ T cell subsets and the 427 genes associated with CD8$^+$ T cell immune infiltration from turquoise module, shown in supplementary Table 2 for details (Fig. 5A). They are significantly enriched in GO terms such as immune system, leukocyte activation, lymphocyte activation and immune response (Fig. 5B). Based on the 112 genes, a prognostic signature model was established using the LASSO algorithm (Fig. 5C), obtaining a formula "Riskscore=-0.041864381*TRIM22-0.036542873*LAG3-0.024487767*SAMD3-0.052887584*SAMSN1", where LAG3 was identified as a negative correlate of the model. The risk score of each sample was calculated based on the formula, and the samples were categorized into the High-risk and Low-risk groups based on the median value (Fig. 5D). In the TCGA-SKCM training set, the OS was significantly better in the Low-risk group ($P<0.001$), and the ROC curves at 1, 3, and 5 years also presented good diagnostic value of the prognostic signature model (Fig. 5E and F). Subsequently, two datasets, GSE54467 and GSE65904, were selected as validation sets for the TRS, and their KM curves indicated that the prognosis of the Low-risk group was significantly better than that of the High-risk group, and the predictive accuracy of the prognostic signature model was verified (Fig. 5G-J). IHC detection results showed that compared with the control group, the expression of LAG3, SAMD3 and SAMSN1 was higher in the model group, and the expression of TRIM22 was lower in the model group (Fig. 5K, L).

Immune infiltration and immunotherapy analyses in SKCM patients

Compared with the High-risk group, the Low-risk group had significantly higher ESTIMATEScore, ImmuneScore, StromalScore, and significantly lower TumorPurity (Fig. 6A). The infiltration of 15 types of immune cells such as B cells memory, Macrophages M2, and T cells CD8 were significantly different between the High-risk and Low-risk groups (Fig. 6B). The expression of immune checkpoint-related genes revealed that the vast majority of immune checkpoints were significantly different between the High-risk and Low-risk groups (Fig. 6C). The immunotherapy sensitivity of patients in the High-risk and Low-risk groups was subsequently analyzed. The results showed that patients in the High-risk group had a higher similarity in expression patterns with patients responding to CTLA-4-nOR inhibitors, and patients in the Low-risk group had a higher similarity in expression patterns with patients responding to PD1-R inhibitors (Fig. 6D). In addition, the differences in $\log_2$ (IC50) between the High-risk and Low-risk groups for individual drugs across multiple cell lines in the GDSC2 database were analyzed and the top 6 differential chemotherapeutic agents between the High-risk and Low-risk groups (Fig. 6E).

Miptenalimab and ZYF0033 inhibited SKCM proliferation and metastasis in mice

After subcutaneous injection of melanoma cells, mice exhibited a significant increase in body weight and tumor volume (Fig. 7A). From day 24 after Miptenalimab and ZYF0033 treatment, the rate of increase in body weight and tumor volume of mice was significantly suppressed compared to the DMSO group (Fig. 7B and C). In addition, the tumor size was found to be significantly smaller in both the Miptenalimab and ZYF0033 groups

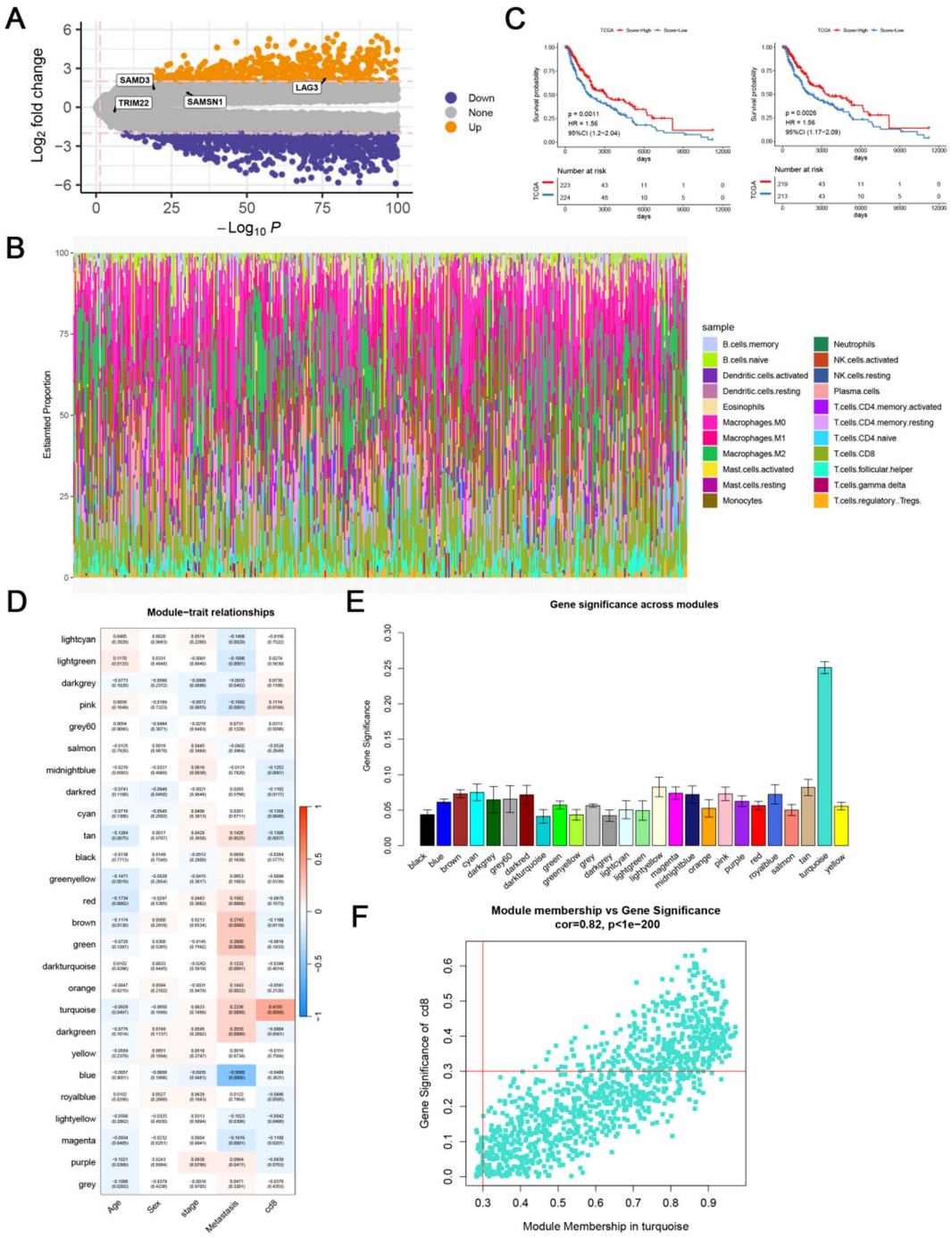

Fig. 4. Differential gene expression analysis and WGCNA. (**A**) Volcano plot of the differential gene expression analysis of TCGA-SKCM samples/GTEX normal control samples; (**B**) stacked plots demonstrated immune cell infiltration in tumors and normal tissues; (**C**) KM curves of the OS and DSS in the Score-High and Score-Low groups; (**D**) A heatmap of the correlation between gene modules and clinical features, the X-axis represents different clinical traits, while the Y-axis represents different color blocks, each defined by gene clustering; (**E**) Bar graph of significance of color modules related to $CD8^{+}$T cells; (**F**) Scatter plot of modular genes, where the horizontal coordinate is the module membership and the vertical coordinate is the gene significance.

than in the Control group (Fig. 7D, E). In vivo imaging results showed that after treatment with Miptenalimab and ZYF0033, the tumor spread in mice was reduced (Fig. 7F). H&E staining results indicated that the level of immune infiltration was lower in the DMSO group, whereas there were more immune cells infiltrated in the Miptenalimab and ZYF0033 groups (Fig. 7G). The Ki67 results showed that the staining range of cell nuclei was significantly less in the Miptenalimab and ZYF0033 groups than in the DMSO group, suggesting that tumor proliferation was slowed down by the drug treatment (Fig. 7H and I). IHC detection results showed

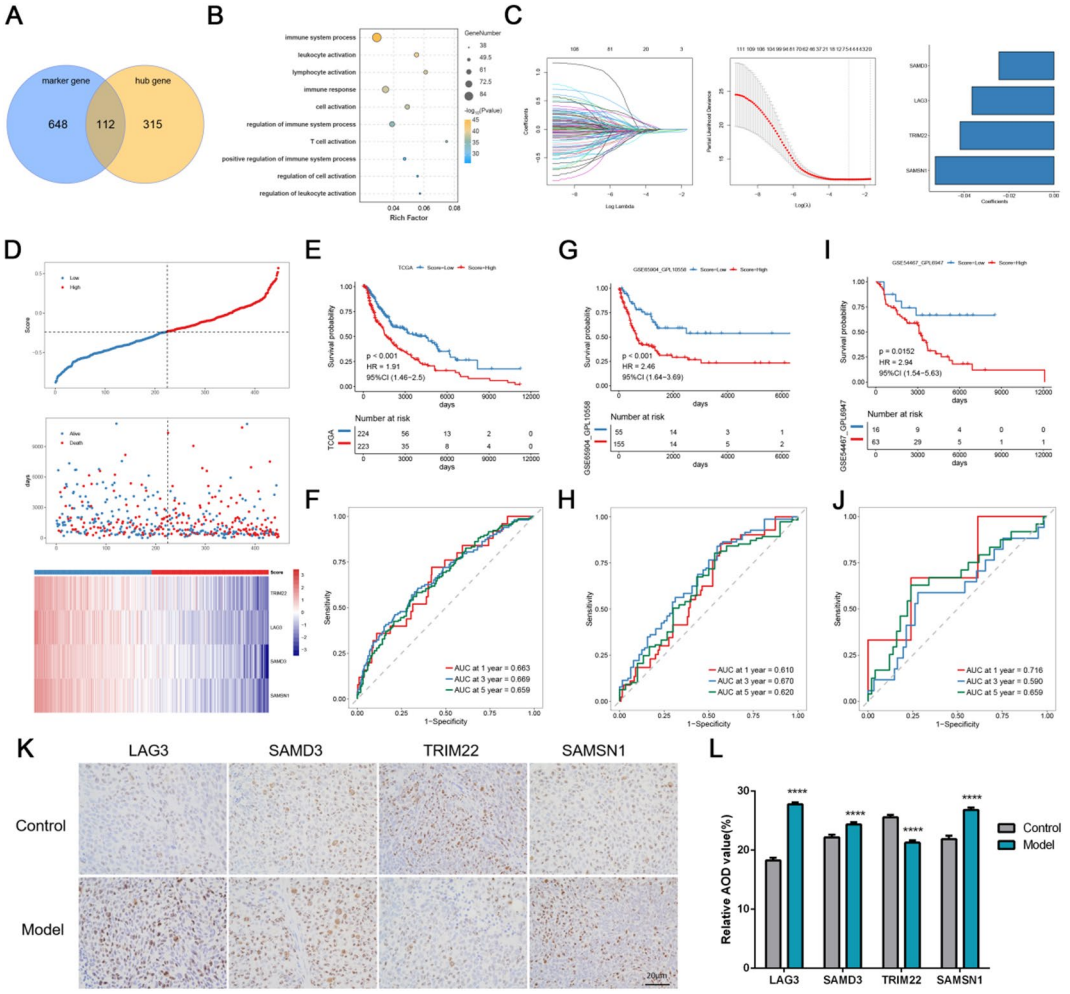

Fig. 5. The TRS of hub genes. (**A**) Venn diagram of intersecting genes; (**B**) GO enrichment analysis results of intersection genes; (**C**) LASSO regression analysis exhibited the trajectory of the LASSO regression independent variables, confidence intervals of Lambda, and LASSO regression coefficients of hub prognostic genes; (**D**) Heatmaps of the risk score profiles and prognostic signature expression in TCGA-SKCM training set; (**E**) KM curves of the TCGA-SKCM training set; (**F**) ROC curves of training set TCGA-SKCM; (**G**) KM curves of validation set GSE65904; (**H**) ROC curves of validation set GSE65904; (**I**) KM curves of validation set GSE54467; (**J**) ROC survival curve of validation set GSE54467; (**K**) Subcutaneously tumor-bearing male BALB/c-nud mice were used to construct the mouse SKCM model. Tumor tissues and adjacent non-tumorous tissues were collected, and IHC was performed to assess the expression of key genes. The scale was set to 20 μm; (**L**) Bar graph of key gene expression, with **** indicating $p < 0.0001$ compared with the control group.

that compared with DMSO group, LAG3 and CTLA-4 expressions were significantly lower in Miptenalimab group and ZYF0033 group, and CD8 expression was significantly higher (Fig. 7J and K). In addition, although Miptenalimab and ZYF0033 have similar therapeutic effects on mice tumors, according to quantitative data, Miptenalimab has a slightly stronger inhibitory effect on the growth of mice tumors than ZYF0033.

Discussion

In the present study, $CD8^+$ $LAG3^+$ T cells and $CD8^+$ $LAG3^-$ T cells were identified by analyzing the three scRNA-seq datasets in SKCM. The responsiveness of $CD8^+$ $LAG3^-$ T cells to SKCM cells was assessed by constructing a prognostic signature model with $CD8^+$ $LAG3^-$ T cell-related genes.

In the TME, increased levels of lymphocyte infiltration were thought to improve the survival of tumor patients[24]. $CD8^+$ T cells are important immune cells in the TME that can specifically recognize a wide range of tumor antigens expressed on tumor cells and exerts cytolytic activity[25]. Assays by Simone L Park et al. have demonstrated that after inoculation of $CD8^+$ T cells, the melanoma-transplanted mice do not exhibit significant skin lesions over a long period of time, while $CD8^+$ T cell depletion can trigger tumor growth in mice with occult melanoma[26]. This result suggests that the recruitment of activated $CD8^+$ T cells in the TME is effective against SKCM. In the present study, immune infiltration analysis of TCGA-SKCM samples revealed a better prognosis in the Score-High group, which is consistent with the findings of Veatch JR et al.[27]. Subsequently, a prognostic signature model based on $CD8^+$ $LAG3^-$ T cell-related genes was constructed, and the model score was identified

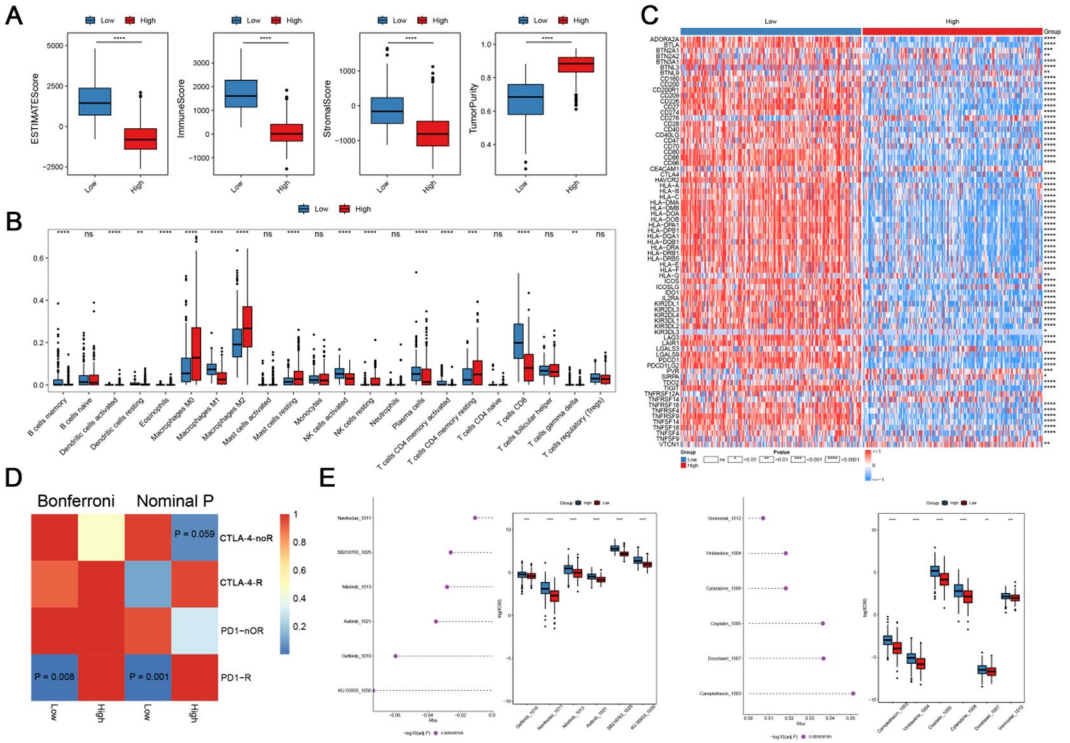

Fig. 6. Immune infiltration and immunotherapy analyses in SKCM. (**A**) Box plots of ESTIMATEScore, ImmuneScore, StromalScore, and TumorPurity between the High/Low-risk groups; (**B**) box plots of immune infiltration levels in the high/low-risk groups; (**C**) heatmap of gene expression of immune checkpoints in the High/Low-risk groups; (**D**) submap analysis showed immunotherapy susceptibility of the High/Low-risk groups; and (**E**) the top 6 differential chemotherapeutic agents between the High/Low-risk groups.

as an independent prognostic factor for SKCM, with patients with high score values having a significantly worse prognosis.

Persistent antigenic stimulation can cause $CD8^+$ T cell depletion and diminish the ability to fight tumor cells. Studies have reported that the mechanism of $CD8^+$ T cell depletion is associated with the overexpression of inhibitory receptors. Naturally, finding targeted drugs that can inhibit receptors has been a research focus. Among the targeted drugs for SKCM, CTLA-4 and PD-1 are often compared, but their mechanisms are distinct. CTLA-4 inhibitors, the first monoclonal antibodies approved for treating advanced SKCM, exert their antitumor effects by enhancing T cell activation and facilitating the differentiation of effector T cells[28]. For PD-1, it is significantly expressed on activated $CD8^+$ T cells and can modulate the antigen-induced immune response[29]. By inhibiting the binding of PD-1 to its ligand, PDL-1, TCR-mediated proliferation and cytokine production can be increased, thereby improving the prognosis of SKCM tumor patients[30]. LAG3 inhibitors are the latest targeted agents approved for the treatment of SKCM. As an inhibitory factor, LAG3 can regulate immune responses by modulating immune cell homeostasis, T cell activation, cytokine production, and other functions[31,32]. In SKCM, LAG3 can suppress the immune microenvironment and thus promote tumor growth[33]. Therefore, LAG3 inhibitors have been developed to block the inhibitory effect of LAG3 on the immune system by specifically binding to LAG3. In this study, CD8 + T cells were characterized by LAG3 and CTLA-4, which may be related to SKCM outcome, and T cell stress state marker gene HSPB1, and the cells were divided into CD8 + LAG3 + T cells and CD8 + LAG3-T cells based on the expression of LAG3. Cell–cell communication analysis was employed to investigate the interactions between two cellular subsets and the melanoma subpopulation. CD8 + LAG3 + T cells, which exhibited stronger interaction with the melanoma cells, were subsequently selected for further analysis.

Clinically, CTLA-4 or LAG3 is usually used in combination with PD1/PDL1 for SKCM treatment, which can provide a better prognosis for patients[34,35]. LAG3 blockade and microwave ablation immunotherapy have also been studied to reprogram TME for anti-tumor purposes[36]. In the present study, LAG3 inhibitors ZYF0033 and Miptenalimab were used to treat SKCM mice. ZYF0033 is a hematopoietic progenitor kinase 1 (HPK1) inhibitor that promotes anticancer immune responses. Miptenalimab exerts its anticancer immune effects by blocking the interaction of LAG3 with its ligand MHC-II. The experimental results showed that both ZYF0033 and Miptenalimab significantly inhibited tumor proliferation and metastasis and increased immune infiltration levels in SKCM mice. The better outcomes of Miptenalimab than ZYF0033 in treating SKCM implied that inhibition of LAG3 expression can effectively prevent melanoma progression, and also reflected that blocking the interaction between LAG3 and its ligands can prevent $CD8^+$ T cell depletion, thus promoting the immune effect. However, unfortunately, the current research on the use of Miptenalimab in the treatment of SKCM is

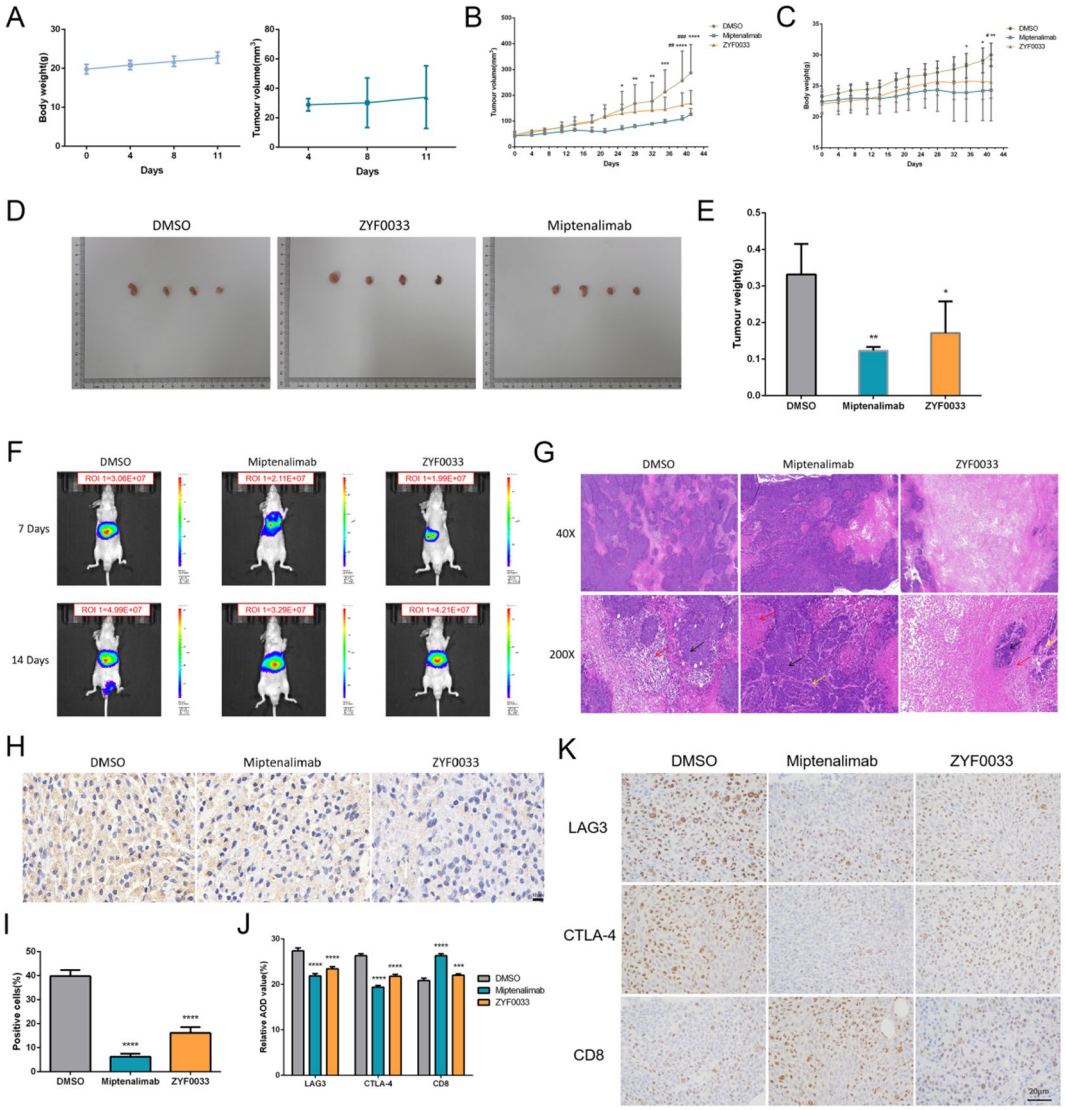

Fig. 7. The therapeutic effects of LAG3 inhibitors and monoclonal antibodies on SKCM in mice. (**A**) Changes in body weight and tumor volume of mice during the modeling process; (**B**) changes in tumor volume of mice in different treatment groups, at which time D0 is the 11th day of drug administration treatment; (**C**) changes in body weight of mice in different treatment groups, at which time D0 is the 11th day of drug administration treatment; (**D**) tumor sizes and weights in different treatment groups; (**E**) Tumor weight of mice in different treatment groups; (**F**) tumor metastasis in vivo in different treatment groups; (**G**) HE staining demonstrated immune cell infiltration in each group; (**H**) Ki67 immunohistochemistry detected tumor proliferation in mice, the scale was set to 10 μm; (**I**) Ki67 quantified histogram of tumor proliferation in mice in each treatment group; (**J**) IHC histogram of LAG3, CTLA-4 and CD8 in each treatment group; (**K**) The expressions of LAG3, CTLA-4 and CD8 in each treatment group were detected by IHC, the scale was set to 20 μm. "*" indicated the significant P value of the DMSO and Miptenalimab groups, with * representing $P<0.05$, ** $P<0.01$, *** $P<0.001$, and **** $P<0.0001$; and "#" indicated the significant P value of the DMSO and ZYF0033 groups, with # representing $P<0.05$, ## $P<0.01$, and #### $P<0.001$.

not extensive, and ZYF0033 seems to show better advantages in this regard. In addition, Miptenalimab is a less mature LAG3 antibody than the FDA-approved LAG3 inhibitor Relatlimab. However, the purpose of selecting Miptenalimab in this study is to evaluate the therapeutic effect of Miptenalimab on SKCM in mice by comparing it with LAG3 inhibitor ZYF0033, providing more possibilities for the treatment of SKCM. However, a larger number of animal samples and more experimental protocols are needed to further evaluate the role and value of Miptenalimab.

Conclusions

In the present study, highly tumor-responsive $CD8^+$ T cell subsets were identified by scRNA-seq, and the tumor responsiveness of SKCM was developed and validated by integrating Bulk RNA-seq. The tumor responsiveness

and prognostic survival of SKCM patients were assessed by the constructed prognostic signature model about $CD8^+$ $LAG3^-$ T cell subsets. Subsequent analyses identified LAG3, SAMD3, SAMSN1, and TRIM22 as prognostic genes associated with SKCM. Research indicates that high levels of LAG3 can lead to progressive impairment of T cell function, but LAG3 inhibitors can restore T cell function in advanced melanoma and enhance anti-tumor immunity[37]. Currently, the roles of SAMD3, SAMSN1, and TRIM22 in modulating T cell function within the context of SKCM remain poorly characterized, with limited relevant literature available. As a result, meaningful comparisons among these genes are not yet feasible. Future investigations will aim to elucidate their contributions to the tumor immune microenvironment in SKCM more comprehensively. In addition, the present study verified the significance of LAG3 on the development of SKCM in mice through in vivo experiments. Immunotherapeutic responsiveness of SKCM could be promoted by inhibiting LAG3 expression or blocking the interaction of LAG3 with its ligands. Therefore, LAG3 has the potential to be a therapeutic target for SKCM.

Data availability

The datasets generated during the current study are available from the corresponding author on reasonable request.

Code availability

Refer to the supplementary file named "code".

Received: 20 February 2025; Accepted: 29 September 2025
Published online: 29 October 2025

References

1. Long, G. V., Swetter, S. M., Menzies, A. M., Gershenwald, J. E. & Scolyer, R. A. Cutaneous melanoma. *Lancet (London England)*. **402** (10400), 485–502 (2023).
2. Brunsgaard, E. K., Wu, Y. P. & Grossman, D. Melanoma in skin of color: part I. Epidemiology and clinical presentation. *J. Am. Acad. Dermatol.* **89** (3), 445–456 (2023).
3. Watts, C. G. et al. Association between melanoma detected during routine skin checks and mortality. *JAMA Dermatology*. **157** (12), 1425–1436 (2021).
4. Tímár, J. & Ladányi, A. Molecular pathology of skin melanoma: Epidemiology, differential Diagnostics, prognosis and therapy prediction. *Int. J. Mol. Sci.* ;**23**(10). (2022).
5. Li, Y. et al. CXCL11 correlates with immune infiltration and impacts patient immunotherapy efficacy: A Pan-Cancer analysis. *Front. Immunol.* **13**, 951247 (2022).
6. Zhang, Y. & Chen, L. Classification of advanced human cancers based on tumor immunity in the microenvironment (TIME) for cancer immunotherapy. *JAMA Oncol.* **2** (11), 1403–1404 (2016).
7. van der Leun, A. M., Thommen, D. S. & Schumacher, T. N. CD8(+) T cell States in human cancer: insights from single-cell analysis. *Nat. Rev. Cancer*. **20** (4), 218–232 (2020).
8. Clemente, C. G. et al. Prognostic value of tumor infiltrating lymphocytes in the vertical growth phase of primary cutaneous melanoma. *Cancer* **77** (7), 1303–1310 (1996).
9. Galluzzi, L., Chan, T. A., Kroemer, G., Wolchok, J. D. & López-Soto, A. The hallmarks of successful anticancer immunotherapy. *Sci. Transl. Med.* ;**10**(459). (2018).
10. Chen, J. et al. Integrated analysis reveals the pivotal interactions between immune cells in the melanoma tumor microenvironment. *Sci. Rep.* **12**, 10040 (2022).
11. Huang, Y., Jia, A., Wang, Y. & Liu, G. CD8(+) T cell exhaustion in anti-tumour immunity: the new insights for cancer immunotherapy. *Immunology* **168** (1), 30–48 (2023).
12. Wang, Z. & Peng, M. A novel prognostic biomarker LCP2 correlates with metastatic melanoma-infiltrating CD8 T cells. *Sci. Rep.* **11**, 9164 (2021).
13. Wang, Y. et al. TNFAIP2 deficiency drives formation of an immunosuppressive tumor microenvironment and confers resistance to anti-PD-1 therapy in skin cutaneous melanoma. *Sci. Rep.* **15**, 25569 (2025).
14. Reina-Campos, M., Scharping, N. E. & Goldrath, A. W. CD8(+) T cell metabolism in infection and cancer. *Nat. Rev. Immunol.* **21** (11), 718–738 (2021).
15. Postow, M. A., Callahan, M. K. & Wolchok, J. D. Immune checkpoint Blockade in cancer therapy. *J. Clin. Oncology: Official J. Am. Soc. Clin. Oncol.* **33** (17), 1974–1982 (2015).
16. Andrews, L. P. et al. Molecular pathways and mechanisms of LAG3 in cancer therapy. *Clin. Cancer Research: Official J. Am. Association Cancer Res.* **28** (23), 5030–5039 (2022).
17. Zarour, H. M. Reversing T-cell dysfunction and exhaustion in cancer. *Clin. Cancer Research: Official J. Am. Association Cancer Res.* **22** (8), 1856–1864 (2016).
18. Yan, M. et al. Single-Cell transcriptomic analysis reveals a Tumor-Reactive T cell signature associated with clinical outcome and immunotherapy response in melanoma. *Front. Immunol.* **12**, 758288 (2021).
19. Kanehisa, M., Furumichi, M., Sato, Y., Matsuura, Y. & Ishiguro-Watanabe, M. KEGG: biological systems database as a model of the real world. *Nucleic Acids Res.* **53**, D672–D677 (2025).
20. Kanehisa, M. Toward Understanding the origin and evolution of cellular organisms. *Protein Sci.* **28**, 1947–1951 (2019).
21. Kanehisa, M. & Goto, S. KEGG: Kyoto encyclopedia of genes and genomes. *Nucleic Acids Res.* **28**, 27–30 (2000).
22. Si, J. et al. Hematopoietic progenitor Kinase1 (HPK1) mediates T cell dysfunction and is a druggable target for T cell-Based immunotherapies. *Cancer cell.* **38** (4), 551–66e11 (2020).
23. Zettl, M. et al. Combination of two novel blocking antibodies, anti-PD-1 antibody ezabenlimab (BI 754091) and anti-LAG-3 antibody BI 754111, leads to increased immune cell responses. *Oncoimmunology* **11** (1), 2080328 (2022).
24. Mihm, M. C. Jr. & Mulé, J. J. Reflections on the histopathology of Tumor-Infiltrating lymphocytes in melanoma and the host immune response. *Cancer Immunol. Res.* **3** (8), 827–835 (2015).
25. Harlin, H. et al. Chemokine expression in melanoma metastases associated with CD8 + T-cell recruitment. *Cancer Res.* **69** (7), 3077–3085 (2009).
26. Park, S. L. et al. Tissue-resident memory CD8(+) T cells promote melanoma-immune equilibrium in skin. *Nature* **565** (7739), 366–371 (2019).
27. Veatch, J. R. et al. Neoantigen-specific CD4(+) T cells in human melanoma have diverse differentiation States and correlate with CD8(+) T cell, macrophage, and B cell function. *Cancer Cell.* **40** (4), 393–409e9 (2022).
28. Willsmore, Z. N. et al. Combined anti-PD-1 and anti-CTLA-4 checkpoint blockade: treatment of melanoma and immune mechanisms of action. *Eur. J. Immunol.* **51** (3), 544–556 (2021).

29. Sharpe, A. H., Wherry, E. J., Ahmed, R. & Freeman, G. J. The function of programmed cell death 1 and its ligands in regulating autoimmunity and infection. *Nat. Immunol.* **8** (3), 239–245 (2007).
30. Ahmadzadeh, M. et al. Tumor antigen-specific CD8 T cells infiltrating the tumor express high levels of PD-1 and are functionally impaired. *Blood* **114** (8), 1537–1544 (2009).
31. Ruffo, E., Wu, R. C., Bruno, T. C., Workman, C. J. & Vignali, D. A. A. Lymphocyte-activation gene 3 (LAG3): the next immune checkpoint receptor. *Semin. Immunol.* **42**, 101305 (2019).
32. Goldberg, M. V. & Drake, C. G. LAG-3 in cancer immunotherapy. *Curr. Top. Microbiol. Immunol.* **344**, 269–278 (2011).
33. Shi, A. P. et al. Immune checkpoint LAG3 and its ligand FGL1 in cancer. *Front. Immunol.* **12**, 785091 (2021).
34. Guy, C. et al. LAG3 associates with TCR-CD3 complexes and suppresses signaling by driving co-receptor-Lck dissociation. *Nat. Immunol.* **23** (5), 757–767 (2022).
35. Asrir, A. et al. Tumor-associated high endothelial venules mediate lymphocyte entry into tumors and predict response to PD-1 plus CTLA-4 combination immunotherapy. *Cancer Cell.* **40** (3), 318–34e9 (2022).
36. Shao, D. et al. LAG3 Blockade coordinates with microwave ablation to promote CD8(+) T cell-mediated anti-tumor immunity. *J. Translational Med.* **20** (1), 433 (2022).
37. Wu, R., Zeng, M., Zhang, Y. & He, J. LAG3 immune inhibitors: a novel strategy for melanoma treatment. *Front. Oncol.* **14**, 1514578 (2024).

Author contributions
JG and YZ wrote the main manuscript text and SG, CD, YZ prepared figures. All authors reviewed the manuscript.

Declarations

Competing interests
The authors declare no competing interests.

Ethics declarations
The animal experiments were approved by the Animal Ethics Committee of the Yangtze University. All operating methods were performed in accordance with relevant guidelines and regulations. All methods reported were in accordance with ARRIVE guidelines.

Additional information
Supplementary Information The online version contains supplementary material available at https://doi.org/10.1038/s41598-025-22377-5.

Correspondence and requests for materials should be addressed to J.G.

Reprints and permissions information is available at www.nature.com/reprints.

Publisher's note Springer Nature remains neutral with regard to jurisdictional claims in published maps and institutional affiliations.